

Report on the new EFOSC2 VPH grisms

Ivo Saviane
Lorenzo Monaco

v 1.0 – March 01, 2008

1 Introduction

In January 2008 the ULTRASPEC project delivered two volume-phased holographic grisms (VPHG) to be used with the EFOSC2 optics coupled to their camera. After the ULTRASPEC run, the VPHGs remained property of ESO, and can thus be offered to the community. On February 13-14, and 14-15, 2008 the grisms were tested to assess their suitability for the purpose of scientific measurements. Here we report on the results of our tests. Note that these tests are valid for EFOSC2 at the 3.6m telescope, so some changes are expected when the instrument is moved to the NTT (in particular, the effective field of view).

2 Blue grism

To characterise the grisms the usual set of calibration frames were taken: bias frames, one arc frame, and dome flat-field frames. An example of raw arc and FF frames are shown in Fig. 1: it is evident that the right part of the CCD is not illuminated, because after passing through the VPHG the beam suffers a lateral deviation. This amounts to $84''$, or in other words, the usable field-of-view is reduced to $4'$. Fig. 2 shows a 2-D plot of the lines recognized in the raw arc, and the master arc after rectifying and wavelength calibrating. The frames have been trimmed down to 2021×1411 px (at 1×1 binning). Several lines are found by the search algorithm, of which ten are used for the wavelength calibration, and are shown in Fig. 3. They are also listed in Table 2. The table also shows that the maximum resolution is ~ 3200 at $\sim 4700 \text{ \AA}$, and also that the resolution is degraded at the extremes of the spectral range. Note that the FWHM spans several pixels, so using a $0''.3$ slit one could reach a resolution $R > 5000$. However a resolution of ~ 3000 is close to the theoretical limit, so only an empirical measurement can confirm this. Using these lines the wavelength calibration curve shown in Fig. 4 is obtained. The dispersion is $0.335 \text{ \AA px}^{-1}$, and the spectrum covers the wavelength range from 4441 to 5114 \AA . The highest dispersion of current EFOSC2 grisms is 1 \AA px^{-1} , so the blue VPH grism offers a value three times larger than what is currently available. A plot of the wavelength calibrated arc is shown in Fig. 5.

3 Red grism

An example of raw arc and FF frames are shown in Fig. 6: in this case some reflections are visible in the arc frame, while the fringe pattern redder than 7000 \AA is visible in the FF frame. For the red grism the non illuminated band has a width of $112''$, so the usable field-of-view is only $3'.5$. Fig. 7 shows a 2-D plot of the lines recognized in the raw arc, and the master arc after rectifying and wavelength calibrating. The frames have been trimmed down to 2021×1231 px (at 1×1 binning). Several lines are found by the search algorithm, and 23 of them are used for the wavelength calibration. They are shown in Fig. 8 and listed in Table 3. The table also shows that the maximum resolution is ~ 3400 at $\sim 6600 \text{ \AA}$, and also that the resolution is degraded at the extremes of the

Table 1: Parameters of VPHGs provided by the ULTRASPEC team.

| Grism | lines mm ⁻¹ | λ_{\min} Å | λ_{cen} Å | λ_{\max} Å | $RS^{(a)}$ | Å px ⁻¹ | FWHM Å | bin | slit |
|-------|---------------------------|-----------------------|-----------------------------|-----------------------|------------|-----------------------|-----------|-----|------|
| 475 | 1557 | 4441 | 4777 | 5114 | 3200 | 0.34 | 1.5 | 1 | 0".5 |
| | | | | | 3200 | 0.67 | 1.5 | 2 | 0".5 |
| | | | | | 2200 | 0.67 | 2.1 | 2 | 1" |
| 656 | 1070 | 6047 | 6597 | 7147 | 3400 | 0.55 | 2.0 | 1 | 0".5 |
| | | | | | 3000 | 1.08 | 2.2 | 2 | 0".5 |
| | | | | | 2000 | 1.09 | 3.3 | 2 | 1" |

Notes:

^(a) V. Dhillon (priv. comm.) has found resolutions up to 4000 with the ULTRASPEC camera. We plan to check this possibility with a fine adjustment of the EFOSC2 camera focus during the commissioning time in April 2008.

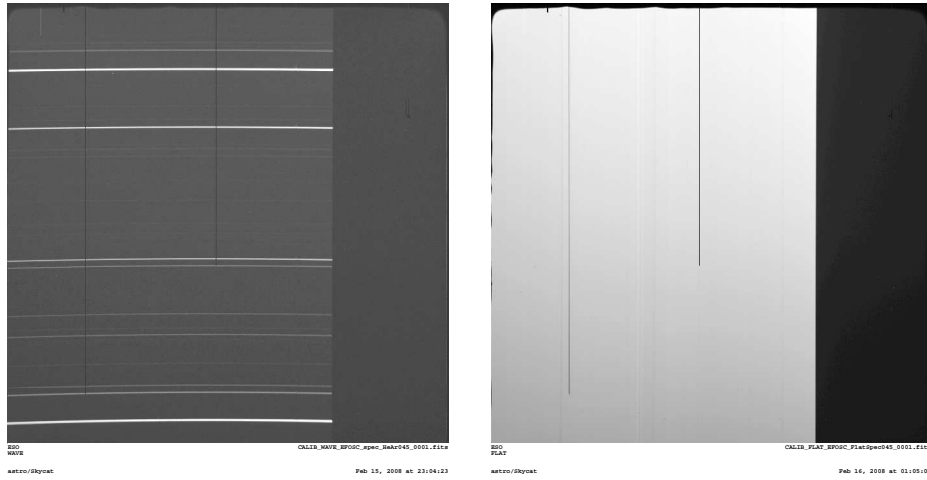


Figure 1: Raw arc and FF of the blue grism

Table 2: For each blue arc line we list its identification and some characteristic parameters. R is the resolution for a 0".5 slit, and n(px) is one FWHM expressed in pixels.

| λ [Å] | ION | FWHM | R | n(px) | COMMENTS |
|---------------|-------|-------|------|-------|---------------------------|
| 4471.4790 | HE I | 2.184 | 2047 | 6.519 | |
| 4510.7334 | AR I | 1.818 | 2481 | 5.427 | |
| 4522.5890 | | 1.748 | 2587 | 5.218 | No stdline at this lambda |
| 4589.8979 | AR II | 1.717 | 2677 | 5.125 | |
| 4628.4409 | AR I | 1.518 | 3049 | 4.531 | |
| 4702.3262 | AR I | 1.471 | 3197 | 4.391 | |
| 4713.1455 | HE I | 1.497 | 3148 | 4.469 | |
| 4921.9312 | HE I | 1.644 | 2994 | 4.907 | |
| 5015.6797 | HE I | 1.800 | 2786 | 5.373 | |
| 5047.7378 | HE I | 2.187 | 2308 | 6.528 | |

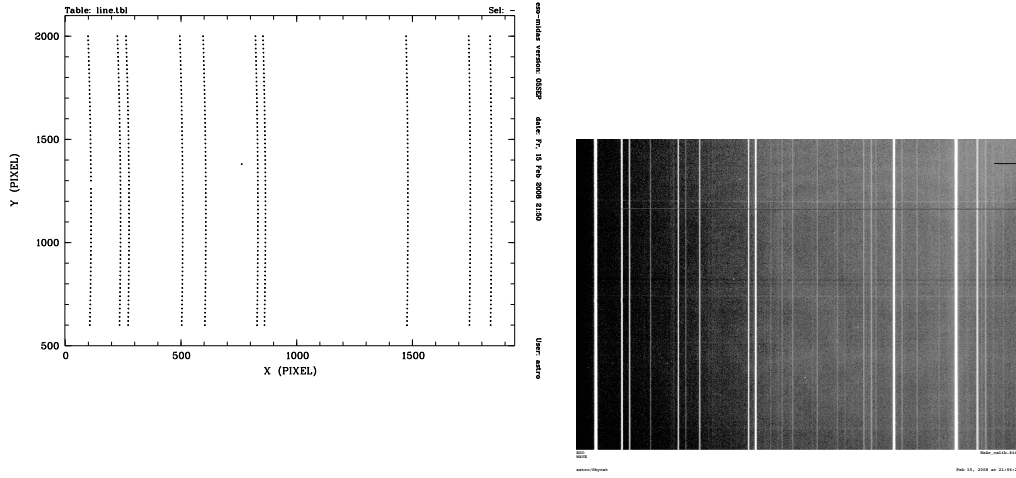


Figure 2: The lines found by the search algorithm on the blue HeAr arc are displayed in the left panel, and the master arc after calibration is shown in the right panel.

Table 3: For each red arc line we list its identification and some characteristic parameters. R is the resolution for a $0''.5$ slit, and $n(\text{px})$ is one FWHM expressed in pixels.

| $\lambda[\text{\AA}]$ | ION | FWHM | R | $n(\text{px})$ | COMMENTS |
|-----------------------|-------|-------|------|----------------|----------|
| 6059.3726 | AR I | 2.134 | 2839 | 3.908 | |
| 6105.6353 | AR I | 2.370 | 2576 | 4.341 | |
| 6145.4409 | AR I | 2.342 | 2624 | 4.289 | |
| 6172.2778 | AR II | | | | sat |
| 6212.5029 | AR I | 2.202 | 2821 | 4.033 | |
| 6296.8721 | AR I | 2.120 | 2970 | 3.883 | |
| 6307.6572 | AR I | 1.985 | 3178 | 3.636 | |
| 6369.5747 | AR I | 1.774 | 3590 | 3.249 | |
| 6384.7168 | AR I | 2.011 | 3175 | 3.683 | |
| 6416.3071 | AR I | 1.988 | 3228 | 3.641 | |
| 6466.5527 | AR I | 1.915 | 3377 | 3.507 | |
| 6538.1118 | AR I | 1.934 | 3381 | 3.542 | |
| 6604.8535 | AR I | 1.999 | 3304 | 3.661 | |
| 6678.1509 | HE I | | | | sat |
| 6752.8335 | AR I | 2.011 | 3358 | 3.683 | |
| 6766.6118 | AR I | 1.997 | 3388 | 3.658 | |
| 6871.2891 | AR I | 2.059 | 3337 | 3.771 | |
| 6937.6641 | AR I | 2.228 | 3114 | 4.081 | |
| 6965.4307 | AR I | | | | sat |
| 7030.2515 | AR I | 2.436 | 2886 | 4.462 | |
| 7065.1899 | HE I | | | | sat |
| 7107.4780 | AR I | 2.802 | 2537 | 5.132 | |
| 7125.8198 | AR I | 2.796 | 2549 | 5.121 | |

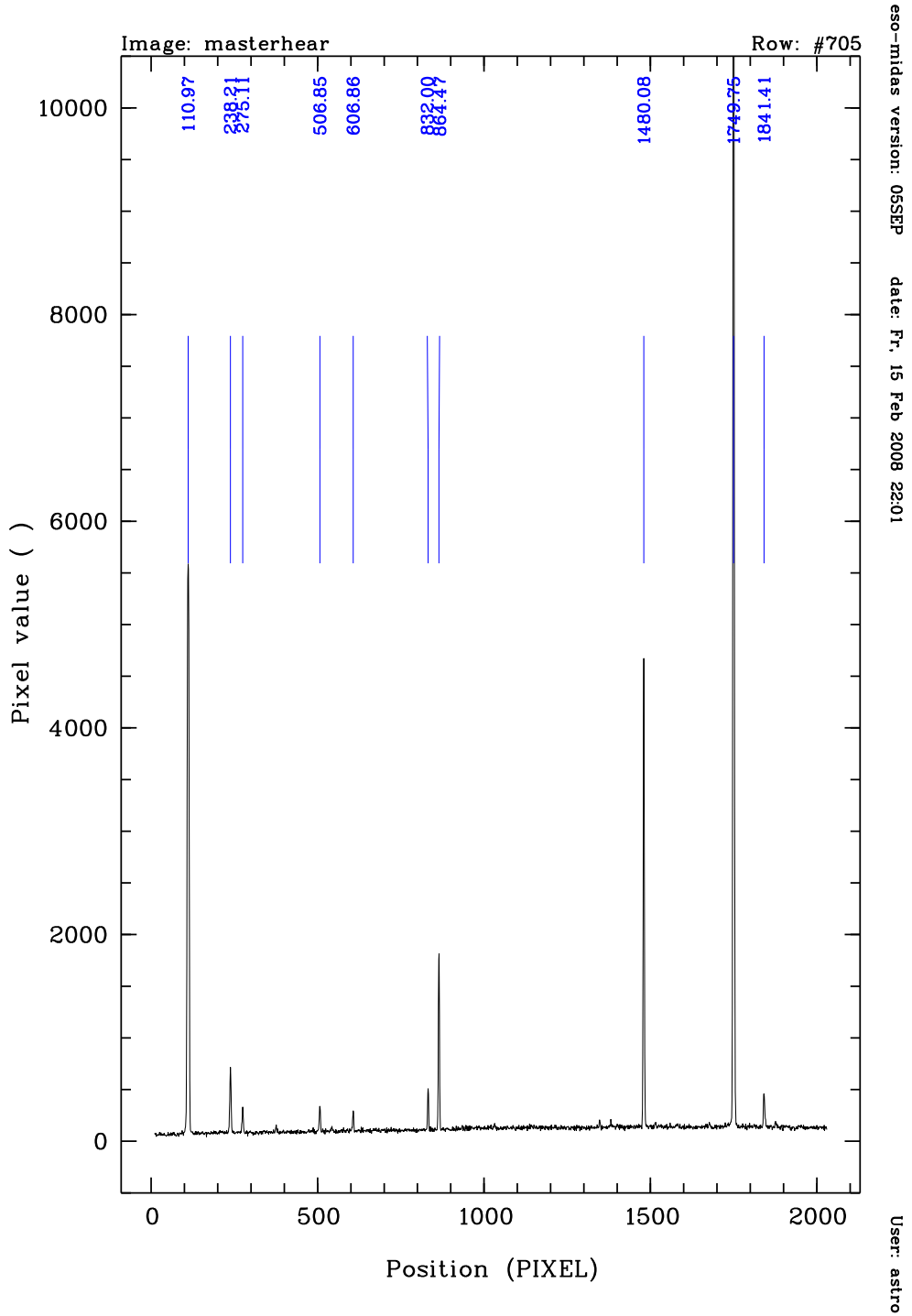


Figure 3: The ten arc lines used for wavelength calibration marked on a trace of the blue arc spectrum.

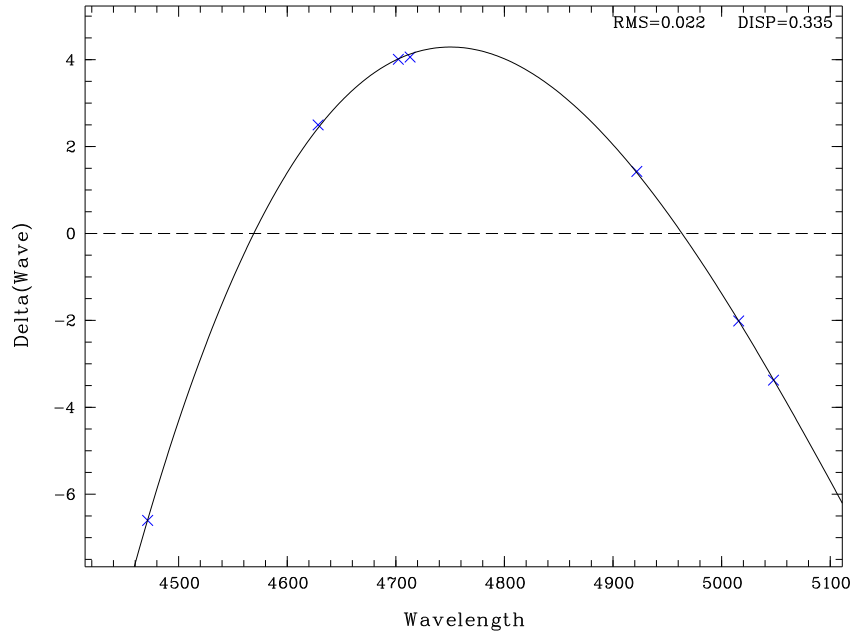


Figure 4: The wavelength calibration curve of the blue VPH grism.

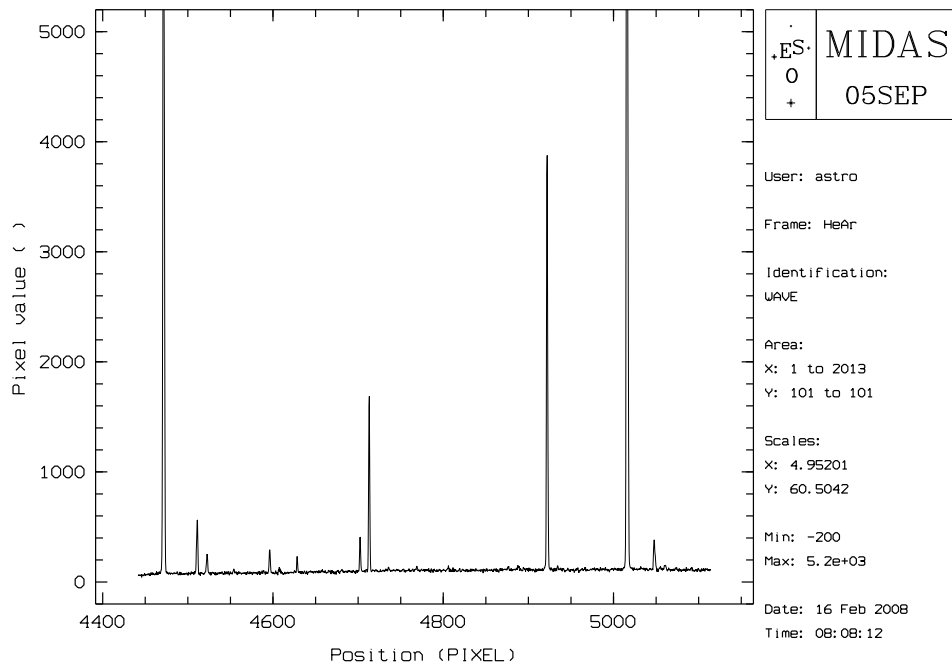


Figure 5: A trace of a blue arc after wavelength calibration

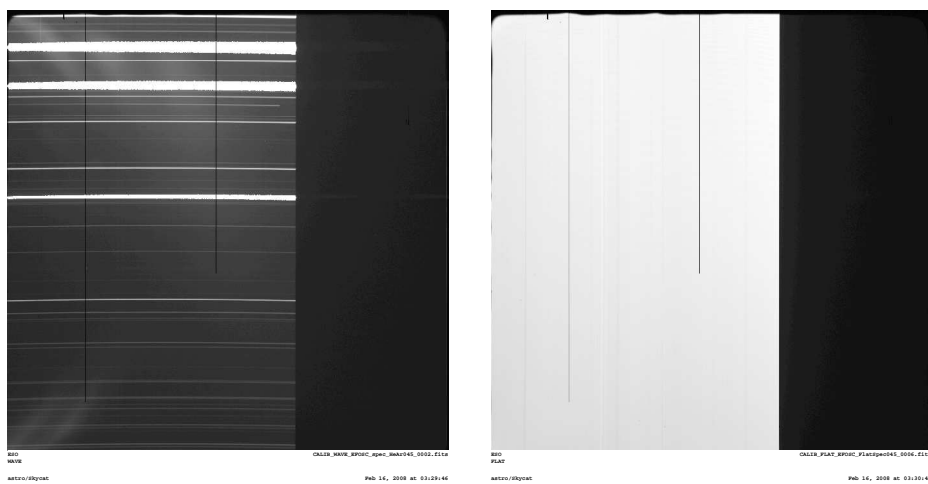


Figure 6: Raw arc and FF of the red grism

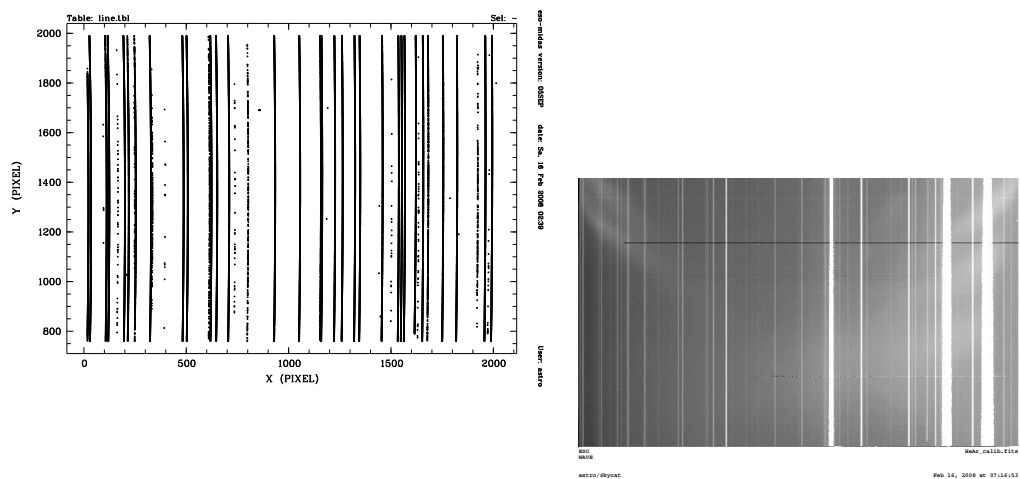


Figure 7: The lines found by the search algorithm on the red grism are displayed in the left panel, and the master arc after calibration is shown in the right panel.

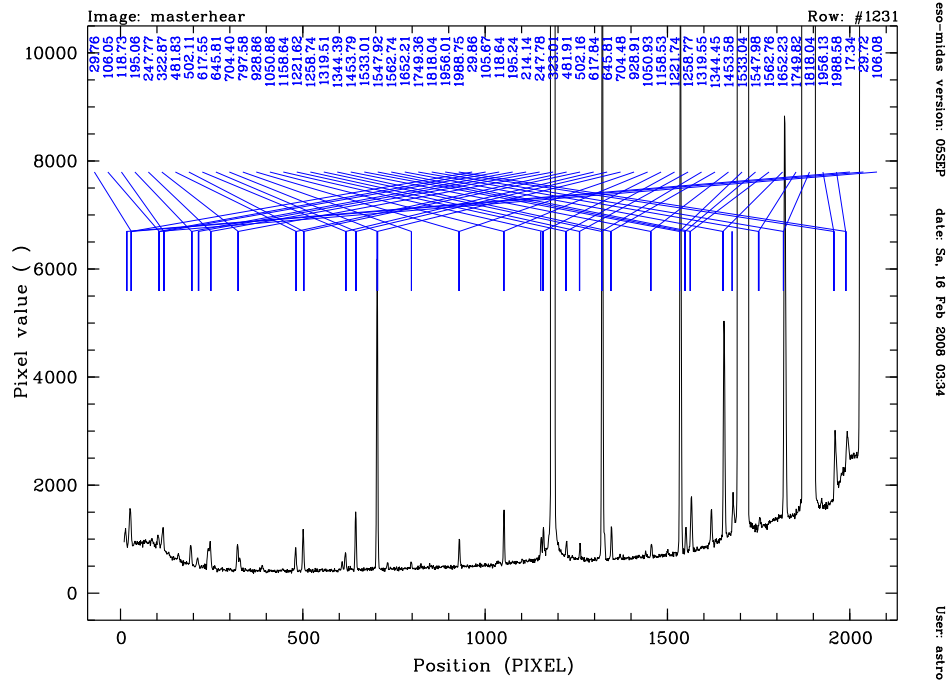


Figure 8: The arc lines used for wavelength calibration marked on a trace of the red arc spectrum.

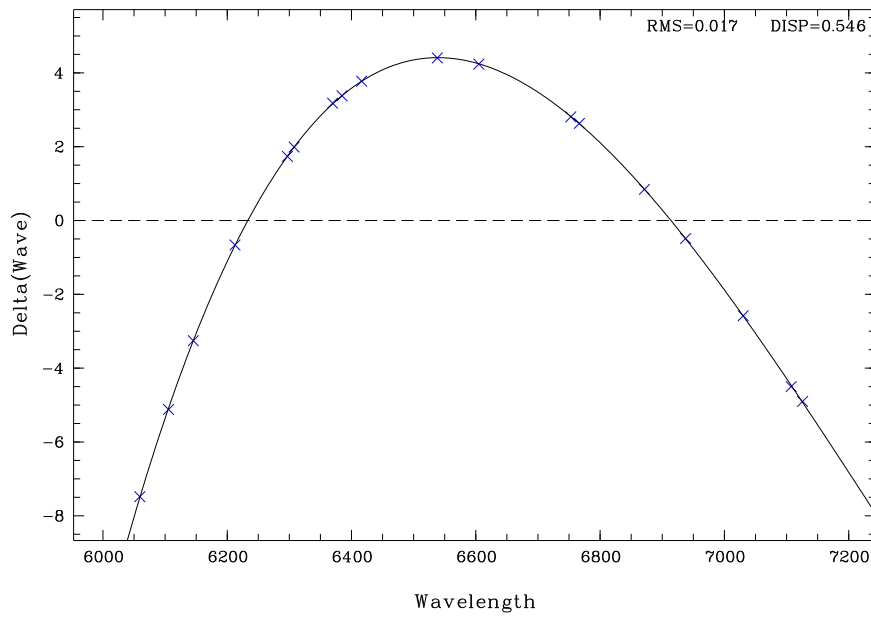


Figure 9: The wavelength calibration curve of the red VPH grism.

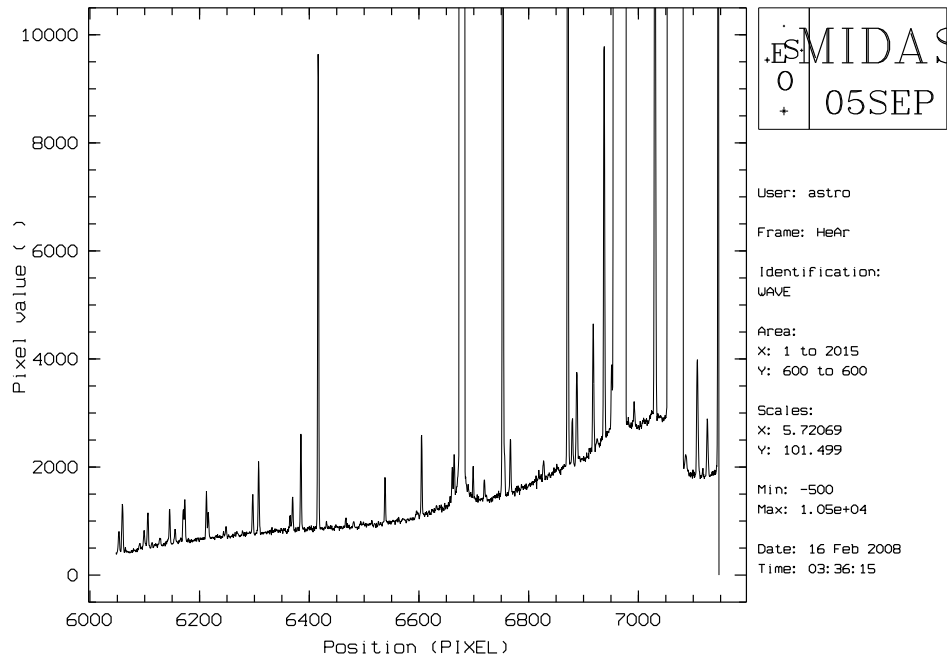


Figure 10: A trace of a red arc after wavelength calibration

spectral range. Note that the FWHM spans several pixels, so using a $0''.3$ slit one could reach a resolution $R > 5000$. However as for the case of the blue grism, an empirical measurement is needed to confirm this guess. Using these lines the wavelength calibration curve shown in Fig. 9 is obtained. The dispersion is $0.546 \text{ \AA px}^{-1}$, and the spectrum covers the wavelength range from 6047 to 7147 \AA . The red VPH grism offers a dispersion value two times larger than that of the highest dispersion conventional EFOSC2 grism. A plot of the wavelength calibrated arc is shown in Fig. 10.

4 Throughput

Unfortunately the two technical nights were not photometric, so no efficiency could be measured. However the grism efficiency could be estimated by the ULTRASPEC team during their observing run. Vik Dhillon (priv. comm.) reported that VPHG 475 is 1.25 times more efficient than grism #3 at 4800 \AA , and that VPHG 656 is 1.3 times more efficient than grism #5 at 6500 \AA . The response functions measured by us are roughly constant across the spectral range, so the quoted efficiencies can be taken as representative of the grisms efficiencies as a whole.

5 A couple of science cases

To see whether the grisms are useful to obtain valuable science data, we took spectra to measure stellar abundances, and the kinematics of spiral galaxies.

5.1 Measurement of lithium line $\lambda 6707.8$

Lithium is a fragile element which is easily destroyed in the stellar interior at relatively low temperatures. As the star approaches the giant phase, the deepening of the convective envelope

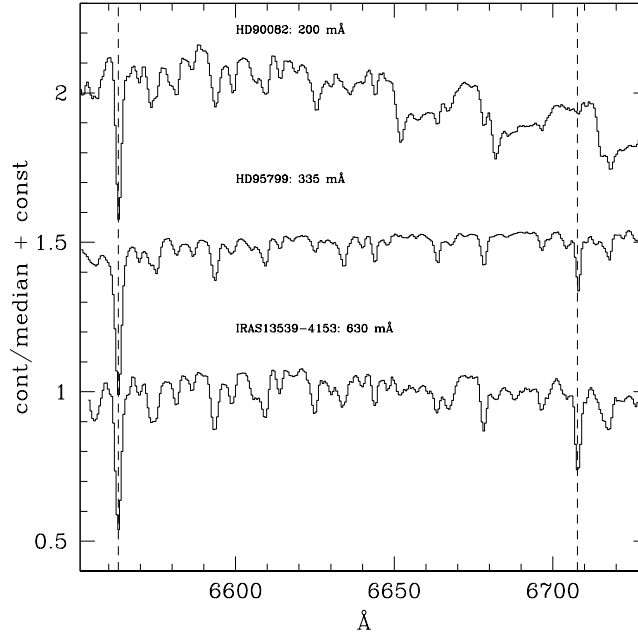


Figure 11: A portion of the spectrum of three stars with different EWs of the lithium $\lambda 6707.8$ line (see the labels above each spectrum). The spectra have been obtained with the red VPHG, and the dashed vertical segments mark the position of $H\alpha$ and the lithium line.

brings to the star surface material which was depleted in Li in the stellar interior. Such mixing of Li-depleted and unprocessed material causes an overall dilution of the Li abundance at the star surface. Assuming that a star is born with a meteoric Li abundance ($A_{\text{Li}} \sim 3.0$ dex), standard models predict that in giants the Li abundance should not exceed ~ 1.5 dex. Yet, about 1–2% of K giants have Li abundances exceeding this value. A few of them even have a Li abundance similar or larger than the meteoric value.

The occurrence of Li-rich stars is usually explained in terms of a Li-production mechanism (i.e. Cameron & Fowler 1971) in the stellar interior associated with a circulation mechanism to bring the produced Li to the star surface. However, a complete theory capable of explaining all the observational facts is still missing and particularly puzzling is the case of low mass star (e.g., Charbonnel & Balachandran 2000, Uttenhaler et al. 2007).

For this reason, in parallel with improving models, data are being collected to construct a more complete observational picture. The Li abundance is routinely measured using the line at 6707.8 \AA . To test the feasibility of such a measurement, we took spectra of three stars with different EWs of the lithium line. The extracted and continuum-normalized spectra are shown in Fig. 11, with SNRs better than 50. Clearly EWs down to 300 m\AA can be easily measured, while the 200 m\AA star is more ambiguous, because of its late spectral type. The line is probably detected, but a confirmation with an earlier type star is needed.

5.2 Rotation curves of spiral galaxies

Rotation curves (RC) of spiral galaxies are used to study their kinematics, in the search for the amount and distribution of dark matter, which are constrained by departures from the expected curve of a rotating disk. These also offer clues on the role of interactions and their impact on evolutionary histories. Galaxy evolution in general can also be explored by comparing rotation curves of distant galaxies with those of nearby objects.

Rotation curves derived from emission lines, and in particular those of $H\alpha$ and $[\text{N II}]$ are

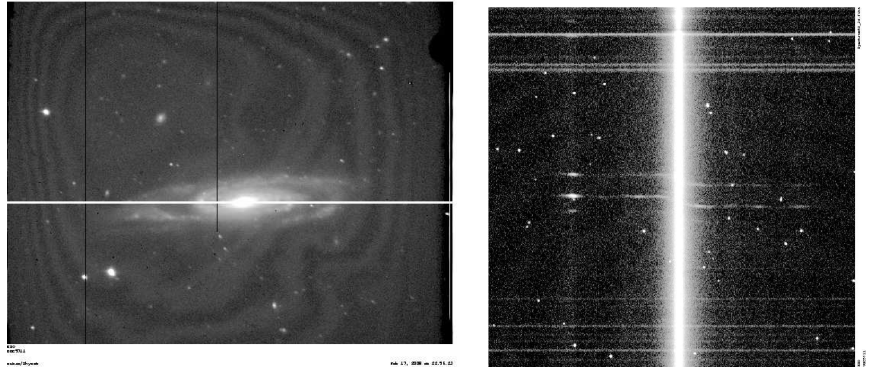


Figure 12: The left panel contains the acquisition image of UGC 5711 in white light, showing the location of the slit across the galaxy. The right panel shows the wavelength-calibrated and distortion-free spectrum in the region of $H\alpha$. The wavelength increases upwards.

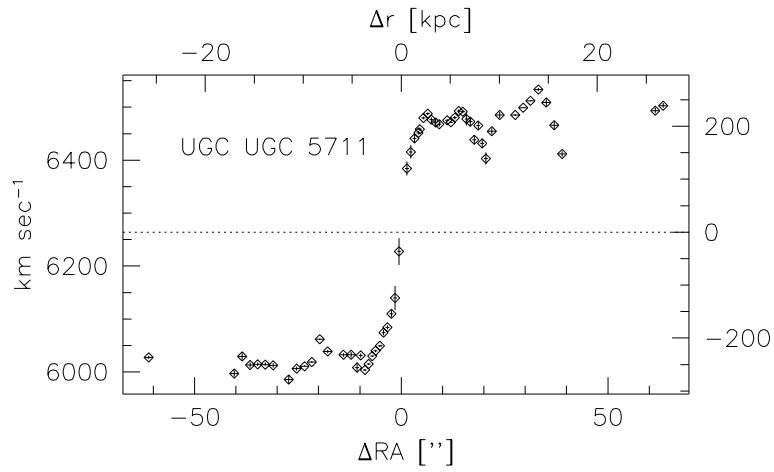


Figure 13: The rotation curve of UGC 5711 measured with the red VPHG. The dotted line shows the recession velocity of 6264 km sec^{-1} from RC3. The physical radius has been computed assuming $H_0 = 72 \text{ km sec}^{-1} \text{ Mpc}^{-1}$.

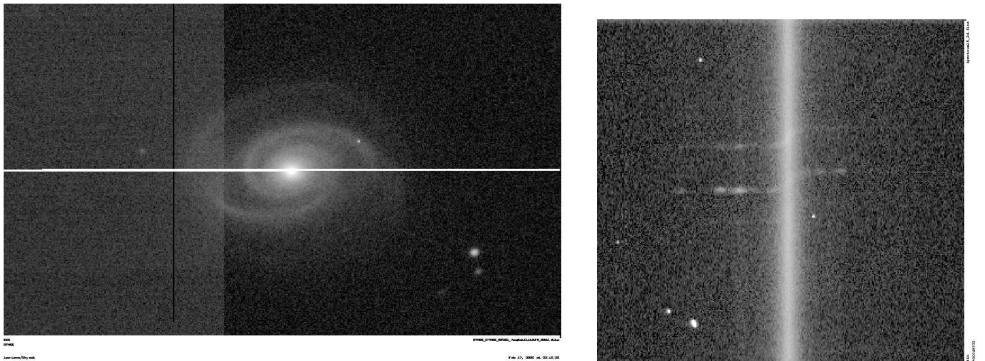


Figure 14: The slit position across PGC 048532 is shown in the R -band acquisition image (left panel), while the right panel shows the wavelength-calibrated and distortion-free spectrum in the region of $H\alpha$. The wavelength increases upwards.

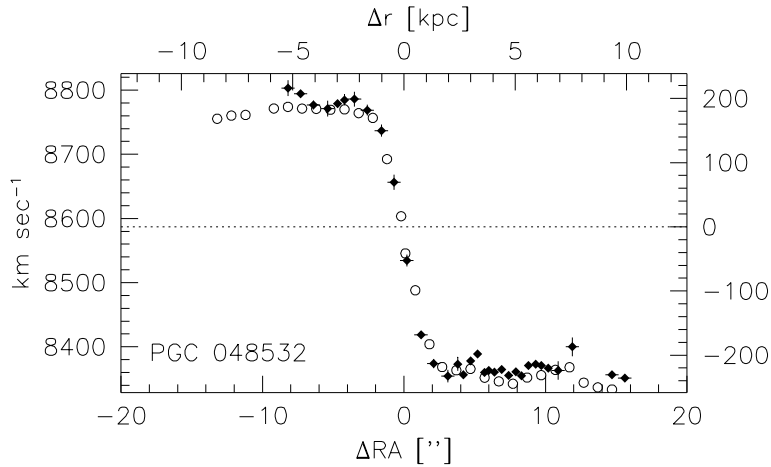


Figure 15: The rotation curve of PGC 048532 measured with the red VPHG (filled diamonds + error bars) compared to the result (open circles) obtained with EMMI by Yegorova et al. (2008). The dotted line shows the recession velocity of 8587 km sec^{-1} from RC3. The physical radius has been computed assuming $H_0 = 72 \text{ km sec}^{-1} \text{ Mpc}^{-1}$.

particularly useful to derive the mass distribution in disk galaxies, because they trace the motion of interstellar gas of the young population. This has a velocity dispersion (of the order of $5\text{--}10 \text{ km s}^{-1}$) that is much smaller than its rotational velocity, allowing accurate measurements. Among spiral galaxies, giant spirals seem to be the best laboratories to study the structure and kinematics (see Fig. 13). They have extended disks and rotational velocities up to $\sim 400 \text{ km s}^{-1}$. Through their rotation curves we can study the cusp/core and angular momentum problems and the DM distribution on the 100 kpc scale.

To measure rotation curves of giant spiral galaxies we took spectra of two objects with the red VPHG. The first piece of data is a 1200 sec spectrum of the giant spiral UGC 5711, with the slit oriented along its major axis (see Fig. 12). A portion of the 2D spectrum near $H\alpha$ is shown in Fig. 12. The differential velocity can be easily seen on the frame, and the rotation curve is plotted in Fig. 13 out to $\sim 30 \text{ kpc}$. The figure shows that the systemic velocity is compatible with that of the RC3 catalog, and that the precision we obtain is comparable to that of standard studies of this kind.

The same exercise was done with PGC 048532, for which the slit position and 2D spectrum of 1200 sec are shown in Fig. 14. The rotation curve is displayed in Fig. 15 and as for UGC 5711, the quality of the data is very good out to 10 kpc . For this galaxy, Yegorova et al. (2008, in preparation) obtained an independent RC with a $2 \times 2000 \text{ sec}$ spectrum collected with grating 6 of the EMMI/REMD arm. The resolution was 4900 with a slit width of $1''$. The resulting RC is shown as a solid curve in Fig. 15. It is clear that the two RCs are consistent with each other, demonstrating the suitability of the red VPHG for this kind of studies. Moreover, the EFOSC2 result was obtained in a 70% shorter exposure time.

6 Conclusions

Two new, medium-resolution gratings are now available for EFOSC2, whose characteristics are summarized in Table 1. We have shown that they are suitable for a range of science cases where high-resolution is not needed, and where the higher efficiency of the two gratings (compared to medium-resolution gratings) is beneficial. To make the best use of the gratings, users must be aware of a few drawbacks as well:

- The flat-fields of both grisms show gradients in the cross-dispersion direction, of the order of $\sim 8 \text{ ADU px}^{-1}$ for the red grism and $\sim 6 \text{ ADU px}^{-1}$ for the blue grism. These gradients are also wavelength-dependent, which means that the response functions depend on the position along the slit. An accurate flux-calibration then requires placing the spectrophotometric standards in different positions across the CCD, or working out corrections to some fiducial response function, based on FFs;
- Second order contamination is apparent in the red grism for $\lambda > 6800 \text{ \AA}$, so it is advisable to use order-sorting filters to cut the blue flux, if flux calibration is an issue for the science case.

Note also that the spectral range of the blue grism does not reach the Mg triplet at 5200 \AA or the G-band at 4300 \AA . On the other hand a movable slit is available, that can be used to shift the spectral range to the blue or to the red. The slit has a width of $1''.5$, so we are planning to fabricate a new movable $0''.5$ slit, or to make a new set of off-center slits to cover a redder or bluer part of the spectrum. The offset should be approximately 6 mm.

Acknowledgements

We thank I. Yegorova and A. Pizzella for computing the kinematic data of the spiral galaxies.